Scalable and Reconfigurable Continuously Tunable Lithium Niobate Thin Film Delay Line Using Graphene Electrodes

Qian Qian Song

***Abstract*—We propose a novel continuously tunable delay line in X-cut lithium niobate thin film driven by graphene electrodes, featuring low power consumption and low half-wave voltage-length product. The use of the graphene electrodes combined with the air slots makes the device quite low power consumption. Our designed device, which has a footprint of 8.9 mm $\times$ 1.9 mm, is capable of providing a continuously tunable delay range from 0 to 100 ps with minimum 3 dB bandwidth of $>$20 GHz. By optimizing the width of the waveguide core and the distance between the graphene and the waveguide core, we can obtain the low power consumption and low voltage - length product $V_\pi L = 1.12$ V·cm at 1550 nm when $w = 2$ μm and $d = 0.3$ μm. In addition, the graphene electrode has negligible light absorption with $w = 2$ μm and $d = 0.3$ μm, the switching power is 151 mW without air slots, and the switching power is 95.36 mW with air slots etching depth of 5.3 μm formed on both sides of the waveguides. And further, the air slots formed on both sides and at the bottom of the waveguides make a low switching power of 2.85 mW.**

***Index Terms*—Integrated optics devices, optical switch, mach-zehnder interferometer, lithium niobate thin film, graphene.**

I. Introduction

LOW power or low half-wave voltage and length product ($V_\pi L$), low loss, fast response, and compact optical delay lines play a vital role in the implementation of optical signal buffering and synchronization in communications and information processing [1], the achievement of real-time imaging in optical coherence tomography [2], and the earth observation in synthetic aperture radar (SAR) [3]. Additionally, they are also key components for microwave photonic filters [4] and optical beamforming [5], [6], [7]. These are typically two methods to realize tunable delay lines. One method is introducing a resonant mechanism, such as a micro-ring resonator, which can provide continuously tunable group delay up to the level of a nanosecond with a very compact size [8], but at the expense of large loss and narrow bandwidth [9]. Although the coupled microring resonators, such as side-coupled integrated spaced sequences of resonators (SCISSORs) or coupled-resonator optical waveguides (CROWs), can solve the above issues, they introduce large losses and commonly require complex tuning strategies [10]. In addition, continuous delay tuning has been demonstrated based on a Mach-Zehnder interferometer (MZI) with a tunable coupler [11]. Another important method is realized by integrating a series of optical waveguide switches and pairs of optical paths with different lengths into a circuit. In this way, the reconfigurable structure can be achieved, and larger bandwidth and finer control of tuning can be provided [5]. Here, optical waveguide switches are vital components to obtain configurability and scalability, hence providing the flexibility of the system [5]. True time-delay line we have recently demonstrated using switches and optical paths integrated on ultra-low-loss silica waveguide. Our structure has an average switching power of $\sim$132.6 mW and insertion loss of $<$2.34 dB [5]. To reduce the switching power further, we have demonstrated a low-power waveguide switch with the switching power of $\sim$3.3 mW based on a large thermo-optic (TO) coefficients polymer waveguide and graphene heater [12]. To make the structure more compact and flexible, we have proposed a continuously tunable delay line based on a high-performance three-dimensional polymer switch driving with graphene heaters [13]. However, the continuously tunable delay range is inversely proportional to the 3 dB minimum delay bandwidth. Integrating a continuously tunable delay line and the discrete tunable delay line is a perfect scheme. In addition, compared to the polymer waveguide delay line, lithium niobate on insulator (LNOI) waveguide delay lines are easier integrated with modulators. This is because lithium niobate ($LiNbO_3$, LN) is widely used in electro-optic (EO) modulators, therefore, LNOI also can be widely used in EO modulators due to the superior EO effect; what's more, LNOI with large refractive index difference is very suitable for compact electro-optic tuning devices [14]. Table I summarizes the configurations and the performance of the aforementioned tunable optical delay lines.

Manuscript received 16 May 2022; revised 23 August 2022; accepted 25 August 2022. Date of publication 30 August 2022; date of current version 5 September 2022. This work was supported in part by the National Natural Science Foundation of China under Grants 62075027, U20A20165, and 61905152, in part by the National Key Basic Research Program of China under Grant 2021YFC2401403, in part by the Major Scientific Research Project of Zhejiang Laboratory under Grant 2019MC0AD02, and in part by the Key R&D Program of Sichuan Province under Grant 2020YFSY0003.

The author is with the Research Institute for Intelligent Sensing, Zhejiang Lab, Hangzhou 311121, China, with the Institute of Information System Engineering, PLA Information Engineering University, Zhengzhou 450002, China and also with the School of Optoelectronic Science and Engineering, University of Electronic Science and Technology of China, Chengdu 611731, China (e-mail: 452344827@qq.com).

Digital Object Identifier 10.1109/JPHOT.2022.3202853

TABLE I
THE PERFORMANCE OF THE AFOREMENTIONED TUNABLE OPTICAL DELAY LINES

Configurations	Delay /Increment (ps)	Power (mW)	$V_\pi L$ (V·cm)	Size (mm^2)	Tuning.
Bragg Grating-Si[3]	200	10	N/A	>15	EO
PhC- GaInP[4]	70	N/A	N/A	~ mm	N/A
MZI- SiO_2[5]	90.2/6	132.6	N/A	429	TO
MZI- Polymer [6]	177/11.8	44	N/A	297.29	TO
MZI-Ring Si_3N_4[7]	920	200	25.47	4.15	EO
MZI-Ring-Si[8]	1280	<13.5	N/A	28.62	TO
Ring-Si[10]	135/1.6	30	N/A	N/A	TO
MZI- InP[11]	125	76.2 mA	N/A	N/A	N/A
3D-MZI Polymer [13]	150	3.6	N/A	136	TO
Current work	100	2.85	1.12	16.91	EO/TO

This paper proposes a novel continuously tunable delay line based on high-performance LNOI switches driven by graphene electrodes. Our designed delay line, which has a compact footprint of 8.9 mm × 1.9 mm, achieves a continuously tunable delay range from 0 to 100 ps over a minimum 3 dB bandwidth of >20 GHz. The proposed device could be operated using the TO and EO tuning, and it has a low power consumption using the TO tuning and a low half-wave voltage and length product ($V_\pi L$) using the EO tuning. Additionally, the device has a large bandwidth with a compact structure. Compared to the previous continuously tunable delay line [13], the bandwidth of our proposed device is nearly four times higher. Besides, compared with our previous scheme [13], the proposed structure footprint is shrunk by 87.56%. By optimizing the width of the waveguide core and the distance between the graphene and the waveguide core, a low half-wave voltage and length product of $V_\pi L = 1.12$ V·cm at 1550 nm when $w = 2$ μm and $d = 0.3$ μm have been obtained. Compared to [15], our proposed scheme's $V_\pi L$ is decreased by 51.3%. Consider that the direct current bias point of the modulator based on the LNOI platform with the TO effect is more stable than with the EO effect [15]. Further, we analyzed the performance of the switch using the TO effect, the air slots on both sides and at the bottom of the waveguide were introduced to reduce the power consumption. The switching power of the switch without air slots is 151 mW, the air slots formed on both sides of the waveguides with air slots etching depth of 5.3 μm make the switch a low power consumption of 95.36 mW. Further, the air slots formed at the bottom of the waveguides make the switch have a very low power consumption of 2.85 mW.

II. DEVICE CONFIGURATION AND DESIGN

The proposed reconfigurable and scalable continuously tunable delay line is schematically shown in Fig. 1, which includes

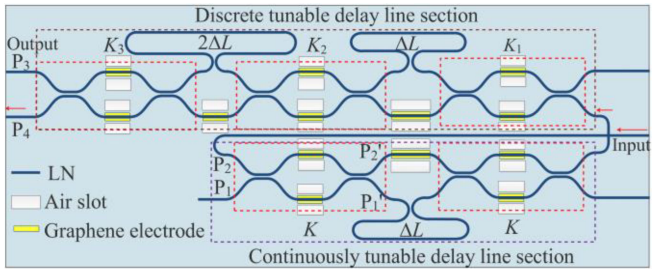

Fig. 1. Schematic of the proposed reconfigurable optical waveguide delay line based on high-performance switches with graphene electrodes. K and K_i (i = 1, 2, 3) are marked above the corresponding switch units bounded by the red dashed box.

a continuously tunable delay line section followed by a 2-bit discrete tunable delay line section. The former includes one delay unit and two switch units, the switch unit in the continuously tunable delay line section is used as a tunable coupler and the power coupling ratios of the two switches, notated as K, the latter includes two delay units and three switch units. The power coupling ratios of three switches, notated as K_1, K_2, and K_3, respectively, as shown in Fig. 1. The switch units include five 2 × 2 MZI switches realized by using a pair of parallel straight waveguide arms to connect two 3 dB directional couplers (DCs) via four sections S-bends.

The continuous tunable delay line section can be operated by continuously varying the power coupling ratios K of two switches from 0 to 1. The switch is constituted of a tunable DC with two 3-dB couplers with length L_c and separation gap G and sandwiched with parallel uncoupled straight waveguides. The graphene electrodes are located on both sides of two arms of the switch unit, acting as a phase shifter, for light path selection. Similarly, the electrodes placed on both sides of the waveguide are used to fine adjust the phase difference in the delay unit. The distance between the graphene electrodes and waveguide is d. Two Gold (Au) pads are connected to each graphene electrode. The cross-section diagrams of the switch with graphene electrodes are shown in Fig. 2(a), 2(b), and 2(c). The material of the waveguide core is LN, which is an X-cut thin film of LN bonded to a layer of silica on a silicon substrate. The corresponding refractive index is 2.1381 at 1550 nm. Therefore, the strongest EO coefficient of LN, i.e., $r_{33} = 30.8$ pm/V, will be efficiently utilized. The lower cladding material is silica with a refractive index of 1.4444, and the silica lower cladding has a height of $h_2 = 5$ μm. The LN waveguides in the switch units have top widths w, a rib height t of 300 nm, and a slab thickness h_1 of 300 nm, and the sidewall of the waveguide is tilted with an angle of 70°. It should be noted that the sidewall tilt angle of 70° corresponds with the state of fabrication technology by inductively coupled plasma reactive ion etching [16], [17].

To reduce propagation loss, the width is tapered up to 4 μm wide in the delay unit, and the propagation loss of a 4 μm wide LNOI waveguide is 0.15 dB/cm [15]. Here we set the effective refractive index of the waveguide in the delay unit as $n_{\text{eff}} = 1.95$. The delay time caused by the first delay unit is set as $\Delta t = 25$ ps. The corresponding length difference of the first delay unit is calculated as $\Delta L = 3846.15$ μm. Therefore, the delay of $2\Delta t$ in

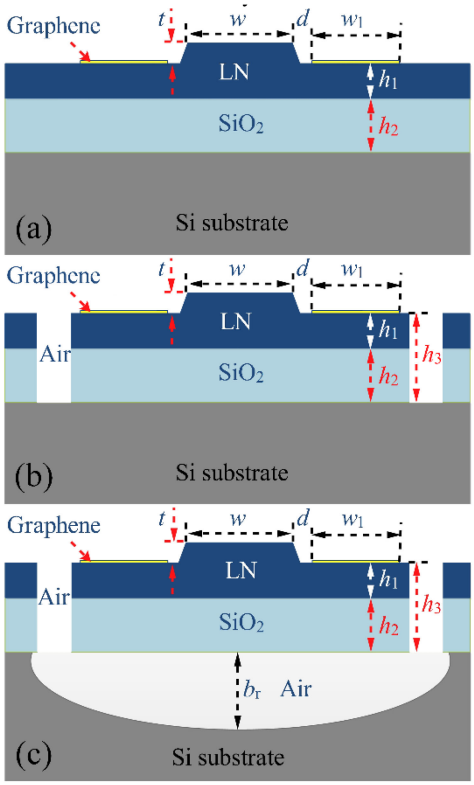

Fig. 2. Cross-sectional diagram of proposed LNOI switch, (a) without air slots on both sides of the MZI arms, (b) with air slots etching depth h_3 on both sides of the MZI arms, (c) with air slots on both sides of the MZI arms and with air slots etching depth b_r at the bottom of the MZI arms.

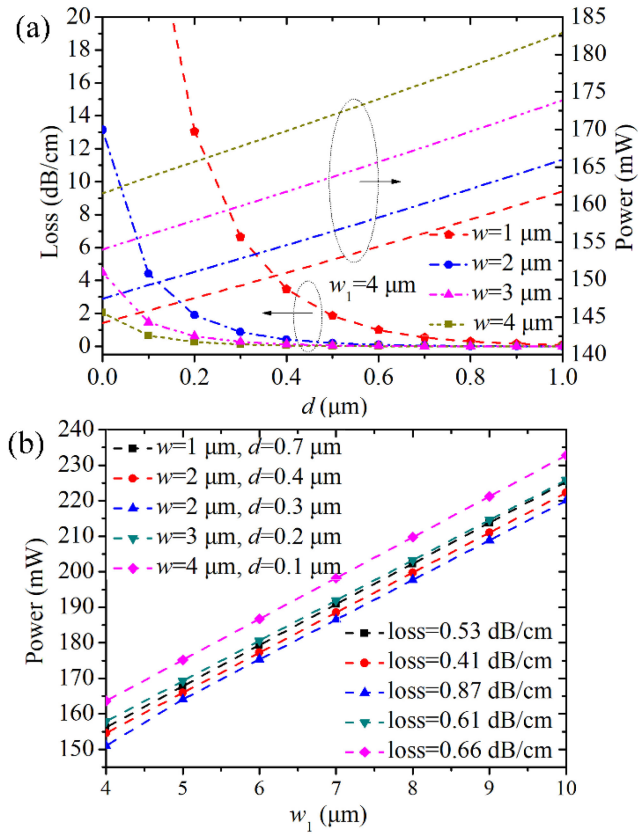

Fig. 3. Calculated electric power applied to the graphene electrode (a) and absorption loss of graphene electrode with different d and $w = 1$ μm, 2 μm, 3 μm, and 4 μm (b) with different w_1 and $w = 1$ μm and $d = 0.7$ μm, $w = 2$ μm and $d = 0.4$ μm, $w = 2$ μm and $d = 0.3$ μm, $w = 3$ μm and $d = 0.2$ μm, and $w = 4$ μm and $d = 0.1$ μm.

the second delay unit is 50 ps, and the corresponding length difference of $2\Delta L$ is 7692.30 μm. We define the maximum delay tuning range of the continuous tunable section as equal to increment delay step $\Delta t = 25$ ps in the discretely tunable delay line section, the corresponding length difference of the first delay unit is calculated as $\Delta L = 3846.15$ μm so that the tuning is continuous over the entire delay range and with large bandwidth. These length differences are realized by constructing semicircular curved waveguides and straight waveguides. The minimum bending radius is set to 150 μm, achieving low bend loss and compact dimension.

III. Switch Characterization

The LNOI switch is the critical component of our proposed scalable and reconfigurable continuously tunable optical waveguide delay time. The LNOI switch utilizes a push-pull configuration, as shown in Fig. 1. Considering the direct current bias point based on the LNOI waveguide platform using the EO effect varies with time. Thus, a static voltage consumption can't maintain the EO phase shift of π, which will increase the complexity of the system. To address this issue, an LNOI modulator based on the TO effect has been proposed [15]. Compared to the EO effect, the direct current bias point with the TO effect is very more stable. In this scenario, the TO phase shifter of the LNOI switch consumes static power. Therefore, the switch with TO effect based on the LNOI platform is more stable, and then we also analyzed the performance of the switch with the TO effect. According to the TO effect, the switching function is realized by tuning the refractive index difference between two arms by adjusting the electric power of the electrodes placed on one side of the MZI arms. When no electric voltage is applied to the graphene electrode, the output optical signal emerges at the cross-state; when a suitable electric current is applied to the graphene electrode, the signal light is switched from cross-state to bar state. Here absorption loss and power consumption are two essential properties of the proposed schemes, which need to be carefully considered in the design process. To realize low power consumption and low absorption loss, parameter d needs to be designed in great detail.

The temperature distribution in the cross-section of the MZI arm could be calculated with COMSOL, as such the power consumption could be obtained. Besides, the absorption loss of graphene electrodes also can be calculated with COMSOL. In addition, the waveguide width w and d affect the performance parameters of the switch, such as the power consumption and the absorption loss. The curves of the absorption loss and power consumption of one LNOI switch against d with widths w of 1 μm, 2 μm, 3 μm, and 4 μm are depicted in Fig. 3(a). It shows that the power consumption decreases when d or w decreases. However, the absorption loss increases when d decreases or w

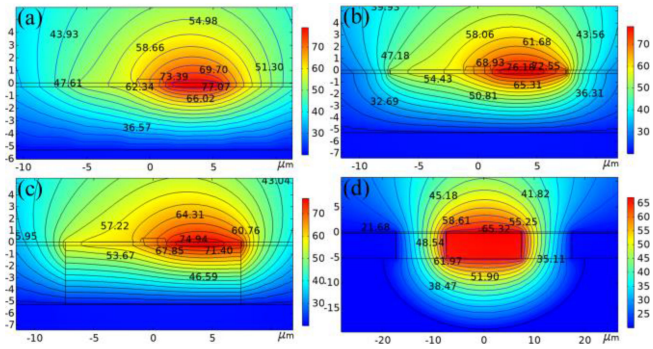

Fig. 4. Calculated temperature distributions with the graphene electrodes having a thickness of 0.35 nm, a width of 4 μm, and a length of 0.5 mm, where the lower cladding has a thickness of 5 μm and different air slots etching depth h_3 and air slots etching depth b_r at the bottom, and an electric driving power of (a) 151 mW with $h_3 = 0$; (b) 118.73 mW with $h_3 = 0.3$ μm; (c) 95.36 mW with $h_3 = 5.3$ μm; (d) 2.85 mW with $b_r = 14$ μm.

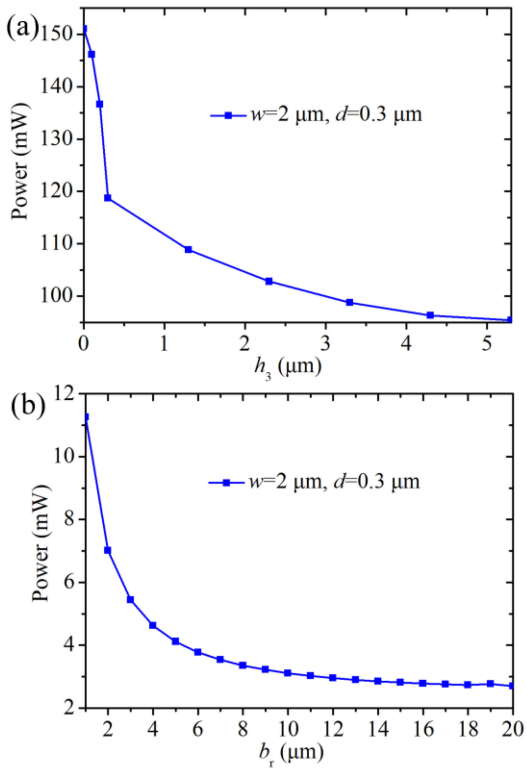

Fig. 5. The relationship between power and air slots etching depth (a) h_3 on both sides (b) and b_r at the bottom with $h_3 = 5.3$ μm.

increases. Further, to obtain the optimal waveguide structure parameters, it is necessary to limit the absorption loss to less than 1 dB/cm to obtain the corresponding w and d. The power consumption of the proposed LNOI switch against w_1 with different w and d is shown in Fig. 3(b). It should be pointed out that the power consumption is a linear relationship with the width of the electrode, and the larger the electrode width, the greater the power consumption. Considering too narrow electrode width w_1, although the power consumption is small, it is easy to fuse, and the optimum parameter is chosen as $w_1 = 4$ μm. Considering that the smaller the power consumption, the better. The optimum parameters are chosen as $w = 2$ μm and $d = 0.3$ μm. In this condition, the lowest power consumption is 151 mW. It should be noted that the switching power of 151 mW is the result without the air slots.

To improve the heat utilization efficiency and reduce the electric power consumption, two air slots on both sides of the graphene electrode are introduced in Fig. 1, as shown in Fig. 2(b). Besides, the air slots at the bottom of the LNOI waveguide in the MZI arm section are introduced in Fig. 1 as shown in Fig. 2(c) to improve the heat utilization and reduce the electric power consumption further. Assuming that the TO coefficient of the LN material is set at 3.7×10^{-5}/K, thermal conductivities of the LN material and the silicon substrate are set at 38 W/(m·K) and 163 W/(m·K), respectively, and the graphene electrode has a thickness of 0.35 nm, a width of 4 μm, and a total length of 0.5 mm, where the graphene is modeled as a conductive boundary with a complex surface conductivity of $6.084 \times 10^{-5} - 7.519 \times 10^{-6}$i [12], when the applied electric power and depth are set as 151 mW with $h_3 = 0$, 118.73 mW with $h_3 = 0.3$ μm, 95.36 mW with $h_3 = 5.3$ μm, 2.85 mW with $b_r = 14$ μm, the corresponding temperature distributions are calculated at an ambient temperature of 20 °C, as displayed in Fig. 4(a)–(d), respectively. The electrical power of 151 mW with $h_3 = 0$, 118.73 mW with $h_3 = 0.3$ μm, 95.36 mW with $h_3 = 5.3$ μm, and 2.85 mW with $b_r = 14$ μm correspond to π phase change and hence the switching power consumption. The relationship between power consumption and air slots etching depth h_3, as shown in Fig. 5(a). From Fig. 5(a), we can see that the power consumption decreases when the slot depth increases. The minimum power consumption is 95.36 mW when $h_3 = 5.3$ μm. The relationship between power consumption and air slots depth b_r at the bottom of the LNOI waveguide, as shown in Fig. 5(b). It could be seen that, as the slot depth b_r at the bottom increases, the power consumption decreases and gradually becomes stable. The optimized power consumption is 2.85 mW when $b_r = 14$ μm. Compared to the first scheme without air slots, here the use of the air slots on both sides and at the bottom reduces power consumption by 98.1%. It should be pointed out that the air slot at both sides and the bottom could be realized and have been realized in a micro-ring resonator based on an LNOI platform [18]. Our proposed device could be fabricated as follows. Firstly, the delay line waveguide could be patterned with a waveguide mask by photolithography technology, then transferred into LN thin film by inductively coupled plasma (ICP) etching technology. Secondly, Au contact leads and pads could be formed using lift-off, that is ~200 nm thick Au film pattern formed by spin-coating, photolithography, sputtering or evaporation coating, and chemical etching processes in turn. Thirdly, the graphene electrodes could also be formed by photolithography, and the specific fabrication process could refer to [12]. Finally, the air slots could be formed by various etching processes to remove the adjacent LN thin film, SiO_2 layer, and silicon substrate around the tuning regions, such as interference arms in switch units.

The field distributions of the fundamental mode superimposed over the waveguide arms at 1550 nm are calculated when the applied electric power and depth are set as 0 mW with

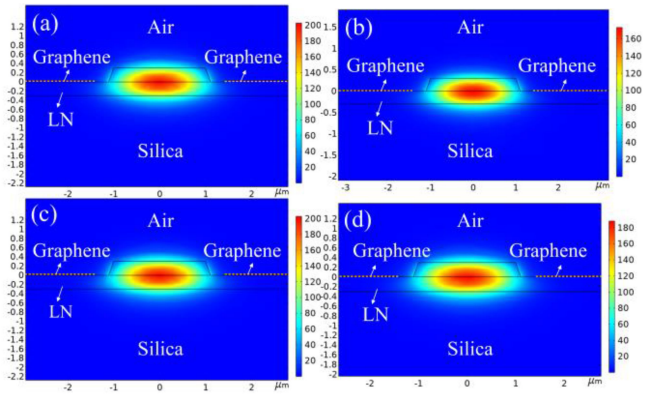

Fig. 6. Cross-sectional diagram of the waveguide arms with the calculated field distributions of the fundamental mode superimposed over the waveguide with the graphene electrodes having a thickness of 0.35 nm, a width of 4 μm, and a length of 0.5 mm at 1550 nm for TE polarization, where the lower cladding has a thickness of 5 μm and different air slots etching depth h_3 and air slots etching depth b_r at the bottom, and electric driving power of (a) 0 mW with $h_3 = 0$; (b) 151 mW with $h_3 = 0$ μm; (c) 95.36 mW with $h_3 = 5.3$ μm; (d) 2.85 mW with $b_r = 14$ μm.

$h_3 = 0$ μm, 151 mW with $h_3 = 0$ μm, 95.36 mW with $h_3 = 5.3$ μm, 2.85 mW with $b_r = 14$ μm, the corresponding filed distributions as displayed in Fig. 6(a)–(d), respectively. From Fig. 6, we can see that the optical field in each case has little overlap with graphene electrodes, which means and could be also calculated that the graphene electrodes have negligible light absorption of <0.088 dB/mm at the OFF and ON states.

To evaluate the performance of our proposed device using the EO coefficient of LN, further, the half-wave voltage-length product ($V_\pi L$) is estimated, we take advantage of the strongest EO coefficient of LN together with COMSOL Multiphysics software on the LNOI platform. Here the switching function is realized by tuning the refractive index difference between two MZI arms based on the EO effect by adjusting the applied voltage on the electrodes placed on both sides of the MZI arms. When no electric voltage is applied to the graphene electrodes, the output optical signal of the MZI switch emerges at the cross-state. However, when a suitable electric voltage is applied to the graphene electrode, the output signal light is switched from cross-state to bar state.

As the gap d between the LNOI waveguide and graphene electrodes will affect the absorption loss of the graphene electrode to the optical signal and $V_\pi L$. The parameter d was devised carefully to balance the trade-off between the absorption loss and $V_\pi L$. The absorption loss of graphene electrodes and $V_\pi L$ could be calculated with COMSOL, and the curves of absorption loss and $V_\pi L$ of one LNOI switch against d with $w = 2$ μm are depicted in Fig. 7(a) . It shows that the $V_\pi L$ decreases when d decreases. However, the absorption loss increases when d decreases. Considering absorption loss and $V_\pi L$, the optimum parameter is $d = 0.3$ μm with $w = 2$ μm. And the corresponding absorption loss <1 dB/cm and $V_\pi L = 1.12$ V·cm. It should be noted that $V_\pi L$ is very small and almost independent of the electrode width.

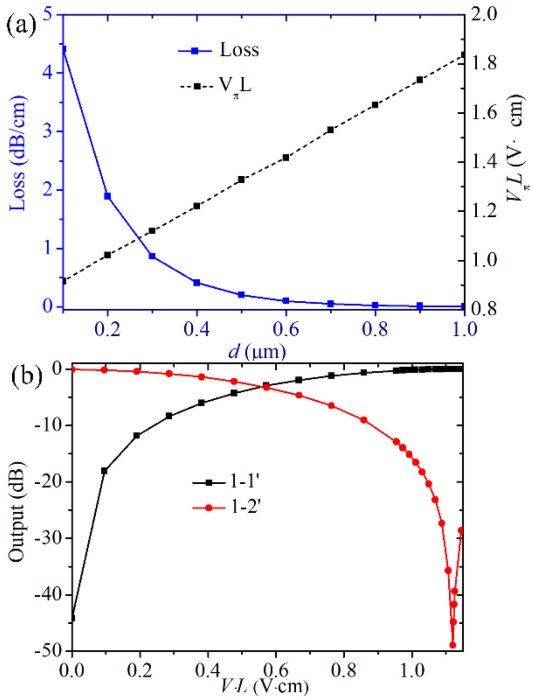

Fig. 7. (a) Calculated absorption loss of graphene electrodes and $V_\pi L$ of the proposed switch for the TE polarization at ON state and 1550 nm wavelength with respect to d; (b) Calculated transmission of the proposed switch for the TE polarization at 1550 nm wavelength with respect to $V \cdot L$.

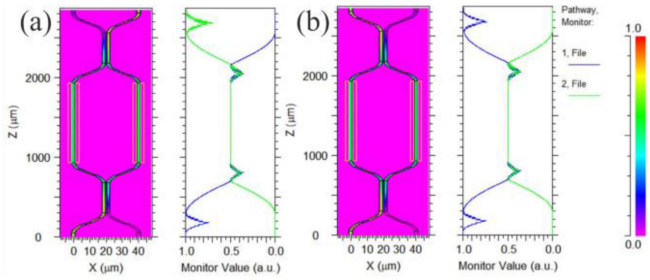

Fig. 8. The calculated transmission of the proposed switch at 1550 nm wavelength for TE polarization at the (a) OFF and (b) ON states.

The LNOI switch parameters can be designed by calculating the light propagating through the MZI with the three-dimensional finite-difference beam propagation method (3DFD-BPM) at 1550 nm. We firstly carried out an extensive simulation on the transmission of DC for 3 dB coupler length L_c with the fixed-width $w = 2$ μm and the gap $G = 0.8$ μm at the OFF state. The optimal length is $L_c = 377.5$ μm. Then, with the parameters designed above, the performances of the proposed LNOI switch over the whole C-band, i.e., from 1530 to 1570 nm, were calculated with Rsoft BeamPROP software for the TE polarization. When the graphene electrodes are applied to suitable voltage V_π (ON state), an appropriate change of the refractive index is introduced to achieve a π phase difference between the two arms, then the light signal launched from P_1 will emerge in P_1', and a tunable coupler can be realized when the voltage V changes continuously from V_π to 0, the corresponding

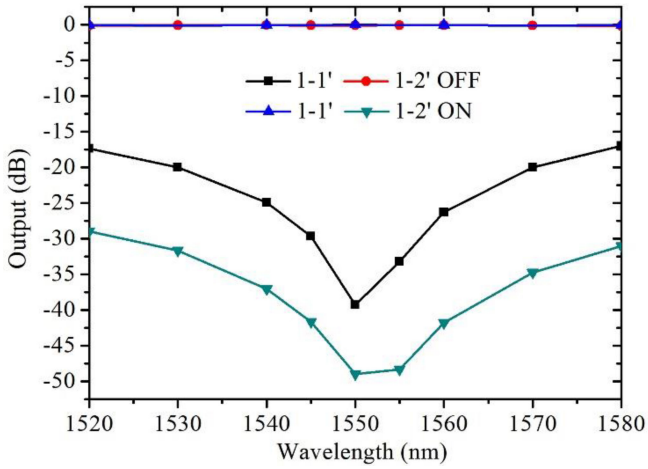

Fig. 9. The calculated transmission of the proposed switch for the TE polarization over the whole C-band at the OFF and ON states.

transmission of the proposed switch at 1550 nm wavelength for the TE polarization with respect to $V{\cdot}L$ is calculated, and as shown in Fig. 7(b). From Fig. 7(b), we also can see that the V_πL is 1.12 V·cm. The calculated transmission when a 1550 nm wavelength light signal is launched into the P_1 port at the OFF and ON states, are shown in Fig. 8(a) and 8(b), respectively. From Fig. 8(a) and 8(b), we can see the output optical signal emerges in P_2' port at the OFF state, and then it will be switched to P_1' port when the electrodes are applied with the switching electric voltage (ON state). It should be noted that when input from the P_2 port, the LNOI switch shows almost the same performance. With the same method, the transmission spectra of the proposed switch over the whole C-band, are calculated and shown in Fig. 9 . It can be seen that the proposed switch can achieve extinction ratios of more than 20 dB over the whole C-band and more than 39.3 dB at 1550 nm wavelength for TE polarization.

IV. Delay Characterization

We assume that the optical signal is launched into input port P_2 of the delay line and finally outputs from the output port P_4. Thus, the delay line was regarded as a single input and single output. To fully understand the influence of the K on the transmission spectrum and delay time of the proposed delay line in detail, we assume the propagation loss is negligible, and introduce the transfer matrix method. The power transfer function of the proposed delay line is

$$|H(\Omega)|^2 = 2K^2 - 2K + 1 - 2K(1-K)\cos(\Omega+\varphi) \quad (1)$$

Here the phase difference $\Delta\phi(\lambda_0) = \Omega + \varphi$. Ω is caused by delay unit length difference ΔL in the continuously tunable delay line section, φ is caused by the graphene electrodes located on the delay unit in the continuously tunable delay line section, and λ_0 is the operating wavelength.

When $K_1 = K_2 = K_3 = 0$, the group delay time is

$$\tau = \frac{K^2 - K(1-K)\cos(\Omega+\varphi)}{K^2 + (1-K)^2 - 2K(1-K)\cos(\Omega+\varphi)} \cdot \Delta t \quad (2)$$

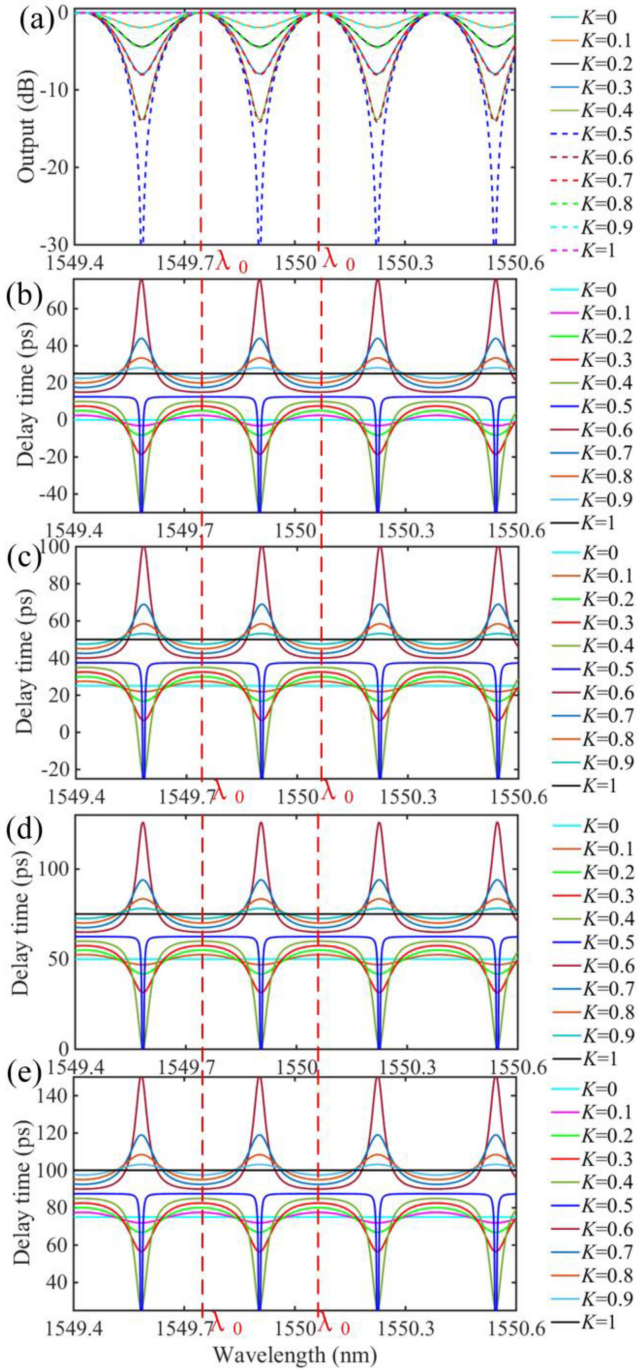

Fig. 10. The calculated (a) transmission spectra (b)–(e) and group delay time of the proposed delay line with different K as a function of wavelength. $\Delta\phi(\lambda_0) = 2N\pi + \pi$, λ_0 is the operating wavelength, and N is an integer. (a) and (b) $K_1 = K_2 = K_3 = 0$; (a) and (c) $K_1 = K_2 = 1$, $K_3 = 0$; (a) and (d) $K_2 = K_3 = 1$, $K_1 = 0$; (a) and (e) $K_1 = K_3 = 1$, $K_2 = 0$.

While if $K_1 = K_2 = 1$ and $K_3 = 0$, the group delay increases by Δt based on formula (2); if $K_2 = K_3 = 1$ and $K_1 = 0$, the group delay increases by $2\Delta t$ based on formula (2); if $K_1 = K_3 = 1$ and $K_2 = 0$, the group delay increases by $3\Delta t$ based on formula (2).

The calculated transfer function and group delay of the proposed delay line with different K as functions of wavelength are

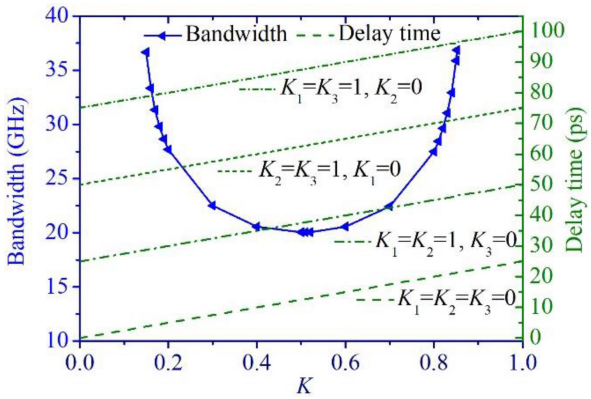

Fig. 11. The calculated group delay time and 3 dB bandwidth of the proposed delay line with different K. $\Delta\phi(\lambda_0) = 2N\pi + \pi$, λ_0 is the operating wavelength, and N is an integer.

shown in Fig. 10, the delay time is linearly dependent on K, and the power transfer function is independent of K and constant when λ_0 satisfies $\Delta\phi(\lambda_0) = 2N\pi+\pi$, N is an integer. Thus, the undistorted signal could output when λ_0 satisfies the above condition. Furthermore, the proposed delay line can provide the continuous tunable range of 0 to 100 ps with $\Delta\phi(\lambda_0) = 2N\pi+\pi$, and the corresponding minimum 3 dB bandwidth of larger than 20 GHz. To illustrate this intuitively, Fig. 11 shows the simulation group delay time and 3 dB operation bandwidth of our proposed delay line as a function of K when λ_0 satisfies $\Delta\phi(\lambda_0) = 2N\pi + \pi$, we can achieve the continuous delay operation and delay range of 0 to 100 ps over the minimum 3 dB bandwidth of >20 GHz. Besides, compared to the continuously tunable delay line constructed with a typical 2 × 2 asymmetric MZI, the minimum bandwidth-delay range product of our proposed device is four times larger than that of the common continuously tunable delay line constructed with a typical 2 × 2 asymmetric MZI using tunable couplers. In addition, for the continuously tunable delay line section, the operating wavelength λ_0 can be tuned within the laser output wavelength range by changing the electric voltage through graphene electrodes above the continuously tunable delay unit until the phase difference $\Delta\phi(\lambda_0)$ between the delay and reference paths is odd times π. Besides, the graphene electrodes placed on the top of the delay unit in the discrete delay line section also can be tuned to solve these issues of large crosstalk in switch units due to fabrication errors, and it can be realized by the method of tuning the corresponding phase difference in discrete delay line section until it is equal to an odd multiple of π. It should be pointed out that the analysis method is similar to [13]. But, most importantly, compared to [13], the bandwidth of the proposed device is nearly four times higher, the proposed structure footprint is shrunk by 87.56%, and it has a lower consumption power and low $V_\pi L$.

Our proposed delay line, which has a compact footprint of 8.9 mm ×1.9 mm, achieves a continuously tunable delay range from 0 to 100 ps over minimum 3 dB bandwidth of >20 GHz. Above all, our proposed configuration could be easily scaled to M bit in discrete delay line section by cascading more delay units and switch units, which conduces to the larger delay time without sacrificing the 3 dB operation bandwidth, here the scalability of the proposed delay line is decided by the refractive index contrast of materials used, propagation loss, and delay time.

V. Conclusion

In summary, we propose a novel scalable and reconfigurable true time delay line based on high-performance LNOI switches driving with graphene electrodes, featuring compact size, low power, low $V_\pi L$, low crosstalk, and large extinction ratio. Our proposed delay line includes a continuously tunable delay line section and a discrete tunable delay line section, which consists of a series of pairs of LNOI waveguides with different physical lengths connected alternately by LNOI switches. The switches, which provide the reconfiguration of the light traveling paths and hence different delays, are based on LNOI MZI structures and driven by graphene electrodes. The use of the graphene electrodes by placing in as close as possible to waveguides combined with the air slots formed on both sides and at the bottom of the waveguides make the switch a quite low $V_\pi L$ and very low power consumption. Our designed delay line, which has a compact footprint of 8.9 mm × 1.9 mm, achieves a continuously tunable delay range from 0 to 100 ps over minimum 3 dB bandwidth of >20 GHz. Compared with our previous scheme [13], the proposed structure footprint is shrunk by 87.56%, and the minimum bandwidth-delay range product of our proposed device is nearly four times higher. By optimizing the width of the waveguide core and the distance between the graphene and the waveguide core, a low half-wave voltage and length product of $V_\pi L = 1.12$ V·cm at 1550 nm when w = 2 μm and d = 0.3 μm have been obtained. Compared to [15], our proposed scheme's $V_\pi L$ is decreased by 51.3%. The extinction ratios are more than 20 dB over the whole C-band and more than 39.3 dB at 1550 nm. Further, the performances of the switch using the TO effect are analyzed, and the air slots on both sides and at the bottom of the waveguide are introduced to improve heat utilization efficiency and reduce power consumption. The switching power of the switch without air slots is 151 mW, the air slots formed on both sides of the waveguides with air slots etching depth of 5.3 μm make the switch a low power consumption of 95.36 mW, and the air slots formed at the bottom of the waveguides make the switch a lower power consumption of 2.85 mW. Our proposed configuration can be easily scaled to M bit in discrete delay line section by cascading more delay units and switch units, which conduces to the larger delay time without sacrificing the 3 dB operation bandwidth. It should be noted that the scalability of the proposed delay line is limited by the propagation loss of the LNOI waveguide and delay time. Our proposed delay line has great potential applications in optical communication systems, microwave photonic systems such as filters and phased array antennas and synthetic aperture radar systems for earth observation.

References

[1] A. E. Willner, B. Zhang, L. Zhang, L. Yan, and I. Fazal, "Optical signal processing using tunable delay elements based on slow light," *IEEE J. Sel. Topics Quantum,* vol. 14, no. 3, pp. 691–705, May/Jun. 2008, doi: 10.1109/JSTQE.2007.914659.

[2] E. Margallo-Balbás, M. Geljon, G. Pandraud, and P. J. French, "Miniature 10 kHz thermo-optic delay line in silicon," *Opt. Lett.*, vol. 35, no. 23, pp. 4027–4029, Dec. 2010, doi: 10.1364/OL.35.004027.

[3] G. Brunetti, D. Conteduca, F. D. Olio, C. Ciminelli, and M. N. Armenise, "Design of an ultra-compact graphene-based integrated microphotonic tunable delay line," *Opt. Exp.,* vol. 26, no. 4, pp. 4693–4704, Feb. 2018, doi: 10.1364/OE.26.004593.

[4] J. Sancho et al., "Integrable microwave filter based on a photonic crystal delay line," *Nat. Commun.*, vol. 3, pp. 1–9, Sep. 2012, doi: 10.1038/ncomms2092.

[5] Q. Q. Song, Z. F. Hu, and K. X. Chen, "Scalable and reconfigurable true time delay line based on an ultra-low-loss silica waveguide," *Appl. Opt.*, vol. 57, no. 16, pp. 4434–4439, Jun. 2018, doi: 10.1364/AO.57.004434.

[6] B. Howley, X. Wang, M. Chen, and R. T. Chen, "Reconfigurable delay time polymer planar lightwave circuit for an X-band phased-array antenna demonstration," *J. Lightw. Technol.*, vol. 25, no. 3, pp. 883–890, Mar. 2007, doi: 10.1109/JLT.2006.890459.

[7] T. Tatoli, D. Conteduca, F. D. Olio, C. Ciminelli, and M. N. Armenise, "Graphene-based fine-tunable optical delay line for optical beamforming in phased-array antennas," *Appl. Opt.*, vol. 55, no. 16, pp. 4342–4349, Jun. 2016, doi: 10.1364/AO.55.004342.

[8] X. Wang et al., "Continuously tunable ultra-thin silicon waveguide optical delay line," *Optica*, vol. 4, no. 5, pp. 507–515, May 2017, doi: 10.1364/OPTICA.4.000507.

[9] J. B. Khurgin, "Dispersion and loss limitations on the performance of optical delay lines based on coupled resonant structures," *Opt. Lett.*, vol. 32, no. 2, pp. 133–135, Jan. 2007, doi: 10.1364/OL.32.000133.

[10] J. Cardenas et al., "Wide-bandwidth continuously tunable optical delay line using silicon microring resonators," *Opt. Exp.*, vol. 18, no. 25, pp. 26525–26534, Dec. 2010, doi: 10.1364/OE.18.026525.

[11] D. Melati, A. Waqas, Z. Mushtaq, and A. Melloni, "Wideband integrated optical delay line based on a continuously tunable Mach-Zehnder interferometer," *IEEE J. Sel. Topics Quantum Electron.*, vol. 24, no. 1, Jan./Feb. 2018, Art. no. 4400108, doi: 10.1109/JSTQE.2017.2723955.

[12] Q. Q. Song, K. X. Chen, and Z. F. Hu, "Low-power broadband thermo-optic switch with weak polarization dependence using a segmented graphene heater," *J. Lightw. Technol.*, vol. 38, no. 6, pp. 1358–1364, Mar. 2020, doi: 10.1109/JLT.2019.2955511.

[13] Q. Q. Song, Z. F. Hu, and K. X. Chen, "Tunable delay line based on high-performance three-dimensional switches using graphene heater," *Appl. Opt.*, vol. 60, no. 9, pp. 2616–2623, Mar. 2021, doi: 10.1364/AO.419697.

[14] X. P. Li, M. K. Wang, J. H. Li, and K. X. Chen, "Monolithic 1×4 reconfigurable electro-optic tunable interleaver in lithium niobate thin film," *IEEE Photon. Technol. Lett.*, vol. 31, no. 20, pp. 1611–1614, Oct. 2019, doi: 10.1109/LPT.2019.2938325.

[15] M. Xu et al., "High-performance coherent optical modulators based on thin-film lithium niobate platform," *Nat. Commun.*, vol. 11, no. 1, pp. 1–7, Aug. 2020, doi: 10.1038/s41467-020-17806-0.

[16] X. P. Li, K. X. Chen, and Z. F. Hu, "Low-loss bent channel waveguides in lithium niobate thin film by proton exchange and dry etching," *Opt. Mater. Exp.*, vol. 8, no. 5, pp. 1322–1327, May 2018, doi: 10.1364/OME.8.001322.

[17] R. Wolf, I. Breunig, H. Zappe, and K. Buse, "Scattering-loss reduction of ridge waveguides by sidewall polishing," *Opt. Exp.*, vol. 26, no. 16, pp. 19815–19820, Aug. 2018, doi: 10. 1364/OE.26.019815.

[18] X. Liu et al., "Highly efficient thermo-optic tunable micro-ring resonator based on an LNOI platform," *Opt. Lett.*, vol. 45, no. 22, pp. 6318–6321, Dec. 2020, doi: 10.1364/ol.415862.